CMS Physics Analysis Summary

Contact: cms-pag-conveners-susy@cern.ch 2013/12/09

Search for top squarks in multijet events with large missing momentum in proton-proton collisions at $\sqrt{s} = 8\,\text{TeV}$

The CMS Collaboration

Abstract

A search for pairs of top squarks decaying to a top quark and a stable, weakly interacting, massive particle is presented. The search selects events containing multiple jets, with at least one identified as originating from a b-quark, and large missing transverse momentum. The search also employs a novel top quark tagging algorithm for identifying a top quark candidate decaying hadronically. It is based on 19.4 fb^{-1} of proton-proton collision data collected at a center-of-mass energy of 8 TeV by the CMS detector at the Large Hadron Collider. The observed event yields are consistent with the SM expectations. Assuming both top squarks decay always into a top quark and a weakly interacting, neutral particle ($\tilde{\chi}_1^0$), the production of top squarks with mass less than 535 GeV is excluded at 95% confidence-level for $\tilde{\chi}_1^0$ masses less than 10 GeV.

1 Introduction

The standard model (SM) of fundamental particles and their interactions has been extremely successful in describing phenomena in the atomic and subatomic realms. The recently discovered boson with a mass of 126 GeV [1, 2] is a prime candidate to be the last particle required in this theory – the Higgs boson. However, a fine-tuned cancellation of large quantum corrections is required in order to stabilize the light Higgs boson mass [3–8]. Supersymmetry (SUSY) is a new symmetry beyond the SM that provides an elegant mechanism to mitigate this hierarchy problem. SUSY proposes a super-partner for each SM particle with the same quantum numbers except for spin, which differs by a half-integer unit. The loop corrections to the Higgs boson mass due to these sparticles are opposite to those of the SM particles [9–13] thus stabilizing the Higgs boson mass. This behavior can survive the breaking of SUSY, which is necessary to explain the non-observation of superpartners with exactly the same mass as their SM counterparts, provided that the superpartners are not themselves too heavy. In particular, the top squark, the SUSY partner of the top quark, may be relatively light (less than ~ 1 TeV) in order for SUSY to provide a natural (not fine-tuned) solution to the hierarchy problem. In addition to solving the problem of radiative stability, some SUSY models are attractive since they also offer a dark matter candidate to explain astrophysical observations [14, 15]. In R-parity conserving SUSY models, the lightest super-symmetric particle (LSP), which is often the lightest neutralino $\tilde{\chi}_1^0$, is weakly interacting, neutral, and stable, thus making it a good dark matter candidate.

Searches for top squark pair production have been performed by the ATLAS Collaboration [16–18] and the CMS Collaboration [19–21] at the LHC and by the CDF [22] and DØ [23] Collaborations at the Tevatron.

This paper presents a search for the direct production of a pair of top squarks ($\tilde{\mathrm{t}}\tilde{\mathrm{t}}^*$) in multijet events with a large imbalance in transverse momentum. The search is based on 19.4 fb^{-1} [24] of proton-proton collision data collected using the CMS detector at the Large Hadron Collider (LHC) at a center of mass energy of 8 TeV. For this search, the top squark mass is assumed to be sufficiently large such that it always decays into a top quark and a weakly interacting particle $\tilde{\chi}_1^0$. The signal process of top squark pair production considered in this search, $\mathrm{pp} \to \tilde{\mathrm{t}}\tilde{\mathrm{t}}^* \to \mathrm{t}\bar{\mathrm{t}}\tilde{\chi}_1^0\tilde{\chi}_1^0$, is represented pictorially in Figure 1.

The analysis strategy consists of utilizing simple and sensitive observables, as well as a selection that mitigates SM backgrounds. The background estimation is based on well-established methods that have been commissioned and used in previous CMS analyses [25–27]. In other words, the search is designed for robustness in the eventuality of a discovery. A central feature of the analysis is the use of a novel top quark tagging algorithm inspired by the one described in [28–30] for increased signal-to-background sensitivity. The residual SM backgrounds after the full selection are predicted with either data driven methods or Monte Carlo based techniques thoroughly validated with collider data.

The targeted decay channel in the search presented in this paper constitutes 46% of the signal events in which both the top and anti-top quarks decay hadronically ($\mathrm{t} \to \mathrm{bjj}$ and $\bar{\mathrm{t}} \to \bar{\mathrm{b}}\mathrm{jj}$). Candidate signal events are selected by requiring five or more jets, no reconstructed electron or muon, at least one jet identified as a b-quark jet, large imbalance in transverse momentum, a reconstructed top quark, and by making several topological requirements. The major SM background contributions to this topology arise from pairs of top quarks, $\mathrm{t}\bar{\mathrm{t}}$, with one of the W bosons from the top quarks decaying into a neutrino and a lepton, Z + jets with the Z boson decaying into a pair of neutrinos, and W + jets with the W decaying into a neutrino and a lepton. Events containing a leptonic decay of a W boson still pass the search selection criteria if the e or μ escapes detection or a τ decays hadronically.

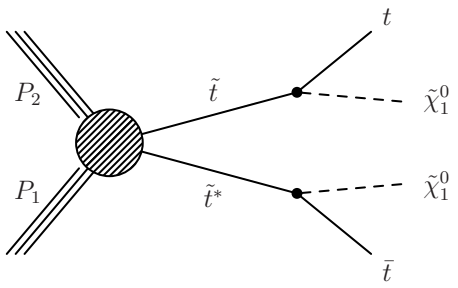

Figure 1: Top squark pair production with the top squark decaying into a top quark and neutralino.

The paper is organized in the following way. Section 2 describes the CMS detector and the event reconstruction algorithms. The production of simulation data is described in Section 3. The dataset and the selection criteria along with the algorithm to reconstruct top quarks are given in Section 4 and estimation of various SM contributions to this signature are described in Section 5. Finally the results are detailed in Section 6 and interpreted in Section 7 and concluding remarks are given in Section 8.

2 Detector and event reconstruction

The CMS detector is a multi-purpose apparatus of cylindrical design with respect to the beams. The main features of the detector relevant to this analysis are described here; more details can be found in Ref. [31]. A polar angle θ is defined with respect to the counterclockwise beam direction. A convenient coordinate is the pseudo-rapidity η, defined as $\eta = -\ln\tan(\theta/2)$. Charged particle trajectories are measured by the silicon pixel and strip tracker, covering $|\eta| < 2.5$. The tracker is immersed in a 3.8 T magnetic field provided by a superconducting solenoid of 6m in diameter that also encircles several calorimeters. The tracker provides resolution of the transverse momentum, represented by p_{T}, of approximately 1.5% for charged particles with $p_{\mathrm{T}} \sim 100\,\mathrm{GeV}$. A lead-tungstate crystal electromagnetic calorimeter (ECAL) and a brass-scintillator hadronic calorimeter (HCAL) surround the tracking volume and cover the region $|\eta| < 3$. A quartz-steel forward hadron calorimeters extend the coverage to $|\eta| \leq 5$. Muons are identified in gas ionization detectors embedded in the steel return yoke of the magnet. The data pertinent to this analysis are recorded using a two level trigger system described in Ref. [31].

The recorded events are reconstructed using the particle-flow algorithm [32]. This algorithm reconstructs charged hadrons, neutral hadrons, photons, muons, and electrons using the information from the tracker, the ECAL and HCAL calorimeters, and the muon system. The $\vec{p}_{\mathrm{T}}^{\,\mathrm{miss}}$ is defined as the negative vector sum of the transverse momentum of all particles reconstructed in the event and $p_{\mathrm{T}}^{\mathrm{miss}}$ is the magnitude of the $\vec{p}_{\mathrm{T}}^{\,\mathrm{miss}}$ vector. All photons and neutral hadrons in an event, but only those charged particles which originate from the primary interaction, are clustered into jets using the anti-k_{T} clustering algorithm with the size parameter 0.5 [33]. Energy from overlapping pp interactions ("pileup"), and from the underlying events, is subtracted using the Fastjet technique [34, 35], which is based on the calculation of the η-dependent transverse momentum density, evaluated on an event-by-event basis. Jet energies are corrected using factors derived from simulation, and, for jets in data, an additional residual energy correction is applied to account for differences in the jet energy scales [36] between simulations and data. Only jets with $p_{\mathrm{T}} > 30\,\mathrm{GeV}$ are used in this search.

For this analysis, a jet is considered a b-quark jet (b-tagged) if it passes the medium working point requirements of the "Combined Secondary Vertex" (CSV) method [37]. The b-quark iden-

tification efficiency is 67% overall and the probability for a jet originating from a light quark or gluon to be mis-identified as a b-quark jet is 1.4%, averaged over p_T in $t\bar{t}$ events [37]. For this analysis, b-tagged jets are required to have $p_T > 30\,\text{GeV}$ and be within $|\eta| < 2.4$.

Muons are reconstructed by finding compatible track segments in the silicon tracker and the muon detectors [38] and are required to be within $|\eta| < 2.1$. Electron candidates are reconstructed starting from a cluster of energy deposits in the ECAL that is then matched to the momentum associated with a track in the silicon tracker. Electron candidates are required to have $|\eta| < 1.44$ or $1.56 < |\eta| < 2.5$ to avoid the transition region between the ECAL barrel and the endcap. Muon and electron candidates are required to originate within 2 mm of the beam axis in the transverse plane.

Events containing a muon or electron with $p_T > 5\,\text{GeV}$ are vetoed based on the spatial distribution of energy deposits around the lepton. A directional isolation Iso^{dir} is defined by considering particles in a region of radius ΔR centered on the lepton direction. A sum is performed on the particle transverse momenta multiplied by the square of the angle in the η-ϕ plane between the particle and the p_T-weighted centroid of all particles contributing to the sum. The weighting enhances the magnitude of the isolation sum for leptons from heavy quark decays, where hadronic activity and the lepton direction are usually closer in η-ϕ space than for leptons from W/Z decays. The ΔR is 0.2 for all muons and 0.2 (0.3) for electrons with $|\eta| \leq 1.44$ (> 1.44). The cut values on Iso^{dir} to decide if a lepton candidate is isolated have been chosen to retain high efficiency, especially for high p_T leptons, and a small fake rate of leptons from b-decays.

3 Monte Carlo event generation

Particle-level simulations of top squark pair signal events with zero, one, and two additional partons are produced using the leading order (LO) matrix element event generator MADGRAPH5 [39] interfaced with PYTHIA 6.4.24 [40]. A CMS custom event tuning [41] (Z2*) is used for parton showering, hadronization, and multiparton interactions in conjunction with the CTEQ6L [42] parton distribution functions (PDF). In the simulation all SUSY particles except $\tilde{t}$ and $\tilde{\chi}_1^0$ are assumed to be very heavy and thus do not affect the signal top-squark production or decay. The top quarks produced in the top squark decays are unpolarized.

Several additional Monte Carlo (MC) samples are used to estimate some of the SM backgrounds as well as to develop and validate methods to estimate backgrounds from data. The $t\bar{t}$ and all three channels of single top quark production samples are generated with the POWHEG [43] program using the CT10 [44] and CTEQ66 [45] parton distribution functions (PDFs), and the W/Z + jets, $t\bar{t}Z$, and $t\bar{t}W$ samples are produced using the MADGRAPH5 [39] event generator program with CTEQ6L PDF [42]. Both programs are interfaced with the PYTHIA 6.4.24 [40] parton-shower, hadronization, and multiparton interaction models. The QCD multijet and diboson (WZ and ZZ) production samples are simulated with PYTHIA 6.4.24 using the CTEQ6L PDF. All the samples are simulated using the Z2* event tune. All the SM background samples, except for the QCD multijet sample, are normalized to the cross sections calculated at next-to-next-to-leading order (NNLO) [46, 47] or approximate NNLO [48–52] in perturbative QCD when available, and otherwise normalized to the cross sections calculated at next-to-leading order (NLO) [53–55].

The generated particle-level events are interfaced to a CMS fast detector simulation [56] for the signal samples and to a GEANT4-based [57] detector simulation for the SM background samples.

4 Event selection and top quark reconstruction

This section describes the dataset and the selection criteria. The central feature of this search is the use of an algorithm to reconstruct hadronically-decaying top quarks and topological cuts using the information from the reconstructed top quark candidates. These are discussed in detail in Sections 4.3–4.4.

4.1 Datasets

The event sample used for this analysis is collected by triggering on events with at least two jets within $|\eta| < 2.6$, online $p_{\mathrm{T}} > 50\,\mathrm{GeV}$, and missing transverse momentum, i.e., online $p_{\mathrm{T}}^{\mathrm{miss}}$, larger than 80 GeV. This trigger is $(98 \pm 1)\%$ efficient for offline $p_{\mathrm{T}}^{\mathrm{miss}} > 200\,\mathrm{GeV}$. Events affected by instrumental effects, particles from non-collision sources, and poor reconstruction quality are rejected [58, 59]. Remaining noise events are also rejected if they contain a jet with $p_{\mathrm{T}} > 30\,\mathrm{GeV}$ in which more than 95% (90%) of the jet's p_{T} is carried by photons (neutral hadrons).

4.2 Pre-selection

The events are required to have:

- no identified and isolated electrons or muons with $p_{\mathrm{T}} > 5\,\mathrm{GeV}$,
- at least five jets with $p_{\mathrm{T}} > 30\,\mathrm{GeV}$ and within $|\eta| < 2.4$ of which the two highest p_{T} jets must have $p_{\mathrm{T}} > 70\,\mathrm{GeV}$ and the next two highest p_{T} jets must have $p_{\mathrm{T}} > 50\,\mathrm{GeV}$,
- at least one b-tagged jet, i.e., $N_{\text{b-jets}} \geq 1$,
- azimuthal angle between the three highest $\vec{p}_{\mathrm{T}}$ jets and the $\vec{p}_{\mathrm{T}}^{\mathrm{miss}}$, $\Delta\phi(\vec{p}_{\mathrm{T}\,j}, \vec{p}_{\mathrm{T}}^{\mathrm{miss}})$ where $j = 1, 2, 3$ is the jet index, larger than 0.5, 0.5, and 0.3 radians, respectively.

The electron and muon vetos minimize the events from $\mathrm{t\bar{t}}$ and W + jets production where one of the W bosons decays into a neutrino and a lepton. No explicit rejection is made to remove events containing a τ-lepton which decays into hadrons. The jet multiplicity and b-tagging requirements help to select signal events since the SUSY signatures of interest tend to have decay products with multiple jets in the central η range and high p_{T} lead jets. The $\Delta\phi$ requirement strongly suppresses the background from QCD multijet events where the $\vec{p}_{\mathrm{T}}^{\mathrm{miss}}$ arises from the mis-measurement of a jet and thus is generally aligned with one of the three highest p_{T} jets.

4.3 Top quark reconstruction

The reconstruction of the hadronically-decaying top quarks is performed in this search as suggested in [28–30]. The analysis reconstructs two top quarks differently, one is "fully-reconstructed" and the other is "partially reconstructed". The requirement for the second top quark is relaxed in order to gain signal acceptance. Once the events with two top quarks are selected, these reconstructed top quarks may be used to form additional topological variables that distinguish between signal and the major background, i.e., the $\mathrm{t\bar{t}}$ background. These topological variables are discussed in detail in Section 4.4.

The collection of five or more jets used in the analysis is divided into all possible sets of three jets and a remnant where the remnant must contain at least one b-tagged jet. The fully-reconstructed top is one of the three jet (tri-jet) combinations. The partially-reconstructed top is then built from the remnant using the b-tagged jet as a seed. The fake rate of the b-tagging is very low; therefore, an identified b-tagged jet indicates another top quark decay around it. If the remnant contains multiple b-tagged jets, the one with the highest p_{T} is used as the seed. To

be considered as a fully-reconstructed top quark, the tri-jet system must satisfy the following requirements:

- each jet must lie within a cone in η-ϕ space of radius 1.5 centered on the momentum direction formed by the tri-jet combination. The radius requirement implies a moderate boost of the top quark as expected for the large $\Delta M = m_{\tilde{t}} - m_{\tilde{\chi}_1^0}$ region targeted in this search.
- the tri-jet system mass ($m^{\text{3-jet}}$) is within 80–270 GeV.
- the tri-jet system satisfies one of the three criteria in Eq. (1) (the jet indices denote an ordering in p_{T} such that $p_{\text{T}}^1 > p_{\text{T}}^2 > p_{\text{T}}^3$).

$$
\begin{aligned}
&\text{a) } 0.2 < \arctan\left(\frac{m_{13}}{m_{12}}\right) < 1.3 \text{ and } R_{\text{min}} < \frac{m_{23}}{m_{123}} < R_{\text{max}}, \\
&\text{b) } R_{\text{min}}^2\left(1+\left(\frac{m_{13}}{m_{12}}\right)^2\right) < 1-\left(\frac{m_{23}}{m_{123}}\right)^2 < R_{\text{max}}^2\left(1+\left(\frac{m_{13}}{m_{12}}\right)^2\right) \text{ and } \frac{m_{23}}{m_{123}} > 0.35, \\
&\text{c) } R_{\text{min}}^2\left(1+\left(\frac{m_{12}}{m_{13}}\right)^2\right) < 1-\left(\frac{m_{23}}{m_{123}}\right)^2 < R_{\text{max}}^2\left(1+\left(\frac{m_{12}}{m_{13}}\right)^2\right) \text{ and } \frac{m_{23}}{m_{123}} > 0.35,
\end{aligned}
\tag{1}
$$

where $R_{\text{min}} = 0.85(m_{\text{W}}/m_{\text{top}})$, $R_{\text{max}} = 1.25(m_{\text{W}}/m_{\text{top}})$, $m_{\text{W}} = 80.4\,\text{GeV}$, and $m_{\text{top}} = 173.1\,\text{GeV}$. The conditions in Eqs. (1.a), (1.b), and (1.c) involving R_{min} and R_{max} are equivalent to the requirements that the m_{23}/m_{123}, m_{12}/m_{123}, and m_{13}/m_{123} are respectively consistent with the m_W/m_{top} ratio. The other conditions are motivated by the Lorentz-structure of the top-W coupling and suppress contributions from light-quark and gluon jets [29]. As demonstrated in Figure 2 for $\text{t}\bar{\text{t}}$ (left) and QCD (right), the conditions in Eq. (1) are very effective for selecting $\text{t}\bar{\text{t}}$ events while rejecting the bulk of QCD events.

If multiple tri-jet combinations satisfy these criteria, the one with $m^{\text{3-jet}}$ closest to m_{top} is selected. The four-momentum of the selected tri-jet system, labeled as $\boldsymbol{p}^{\text{3-jet}}$, is used in the subsequent calculation of topological variables used to refine the event selection and described later.

The partial reconstruction for a possible second top quark is applied in the remnant system, denoted by Rsys. The four-momentum of these identified second top quark candidate decay products, denoted by $\boldsymbol{p}^{\text{Rsys}}$, is used to define the topological variables. The $\boldsymbol{p}^{\text{Rsys}}$ is constructed from either 3, 2, or 1 jet(s) in the Rsys. For the Rsys with ≥ 3 jets, all possible tri-jet combinations containing the b-tagged jet are considered. In order to retain maximum signal acceptance, none of the full reconstruction criteria is applied on the tri-jet combinations. Instead the tri-jet system with $m^{\text{3-jet}}$ closest to m_{top} is selected. In order to reduce the mis-reconstruction of the top quark candidate, the hadronic-decay of the W boson is checked in the selected tri-jet system. If the pair of jets, excluding the b-tagged jet, has a di-jet mass between 50 and 120 GeV, the four-momentum of the tri-jet system is assigned to $\boldsymbol{p}^{\text{Rsys}}$. Otherwise the tri-jet system is discarded and all jet pair combinations involving the b-tagged jet are considered for the remnant system. For this remnant with two jets, it is required that $\Delta R \equiv \sqrt{(\Delta\eta(b,j))^2 + (\Delta\phi(b,j))^2} \leq 2.0$ and that the di-jet mass is less than m_{top}. If multiple jet pairs pass the requirements, the one with smallest ΔR is selected. In this case, $\boldsymbol{p}^{\text{Rsys}}$ is calculated from the four-momenta of the two jets. If no jet pair is found to satisfy the requirements, the b-tagged jet is selected as the complete remnant system, and the four-momentum of this jet is used as $\boldsymbol{p}^{\text{Rsys}}$.

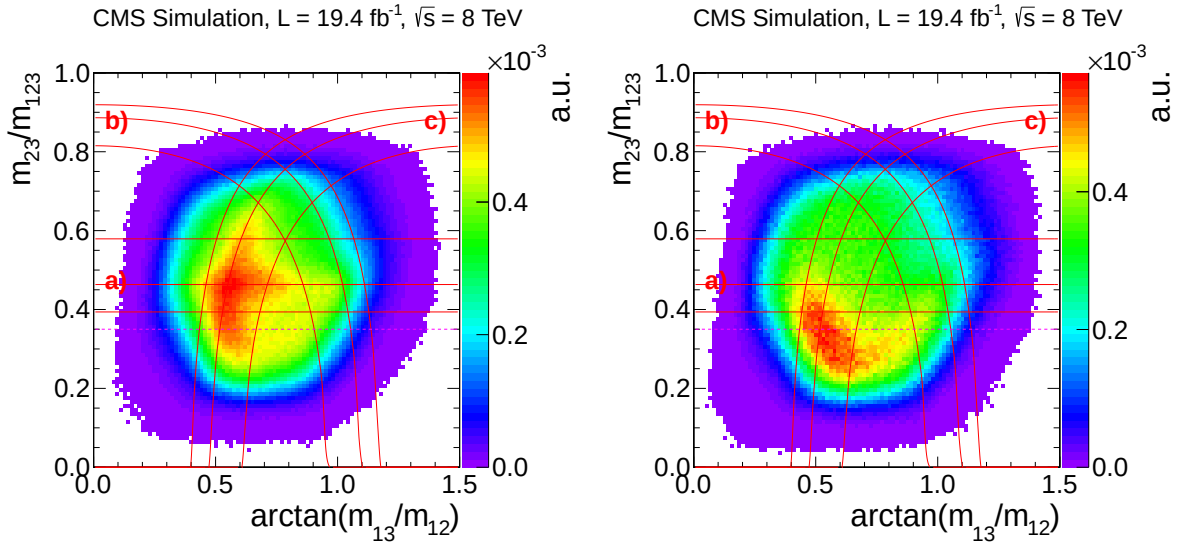

Figure 2: The 2D distributions of m_{23}/m_{123} versus $\arctan(m_{13}/m_{12})$ for $t\bar{t}$ (left) and QCD (right). The three horizontal solid red lines which form a band demonstrate the criteria in Eq. (1.a) with the central line taken as the nominal ratio of m_W/m_{top} and the other two lines showing the boundaries defined by the R_{min} and R_{max}. Similarly the criteria in Eqs. (1.b) and (1.c) are in groups of solid lines. The dashed line indicates the requirement of $m_{23}/m_{123} > 0.35$ as in Eqs. (1.b) and (1.c). All distributions are normalized by the total number of events and the label "a.u." means arbitrary units.

4.4 Topological requirements

After requiring the presence of one fully-reconstructed and one partially-reconstructed top, event topological information is used to distinguish the signal and the SM contributions. In addition to p_T^{miss}, three variables are used: M_{T2}, $M_T^{3\text{-jet}}$, and M_T^{Rsys}.

The variable M_{T2} [60, 61] is an extension of the transverse mass variable that is sensitive to the pair production of heavy particles that each includes an invisible particle in the decay products. The $\boldsymbol{p}^{3\text{-jet}}$ of the fully-reconstructed top quark, the $\boldsymbol{p}^{Rsys}$ of the partially-reconstructed top quark, and the $\vec{p}_T^{miss}$ in an event are used to construct M_{T2} assuming the invisible particles are massless. The top-right plot in Figure 3 shows the M_{T2} shape comparisons between $t\bar{t}$ and some signal points after the pre-selection and a $p_T^{miss} > 200\,GeV$ requirement. For the $t\bar{t}$ background, this variable peaks around the top quark mass and drops rapidly for higher values. For the signal, the M_{T2} distribution peaks higher when the top squark mass is larger than the top quark mass. Since one of the top quarks is only partially reconstructed, the kinematic endpoint of M_{T2} is also only approximately reconstructed.

$M_T^{3\text{-jet}}$ is the transverse mass of the fully reconstructed top quark tri-jet system and the $\vec{p}_T^{miss}$ vector given by

$$(M_T^{3\text{-jet}})^2 = (m^{3\text{-jet}})^2 + 2(E_T^{3\text{-jet}} p_T^{miss} - p_T^{3\text{-jet}} p_T^{miss} \cos\Delta\phi), \quad (2)$$

where $(E_T^{3\text{-jet}})^2 \equiv (m^{3\text{-jet}})^2 + (p_T^{3\text{-jet}})^2$ with $p_T^{3\text{-jet}}$ the magnitude of the $\vec{p}^{3\text{-jet}}$ in the transverse plane and $\Delta\phi$ is the angle between the $\vec{p}^{3\text{-jet}}$ and $\vec{p}_T^{miss}$ vectors in the azimuthal plane. Similarly, M_T^{Rsys} is the transverse mass of the identified partial top decay products in the Rsys and the $\vec{p}_T^{miss}$ vector. The bottom two plots in Figure 3 show the $M_T^{3\text{-jet}}$ and M_T^{Rsys} shape comparisons be-

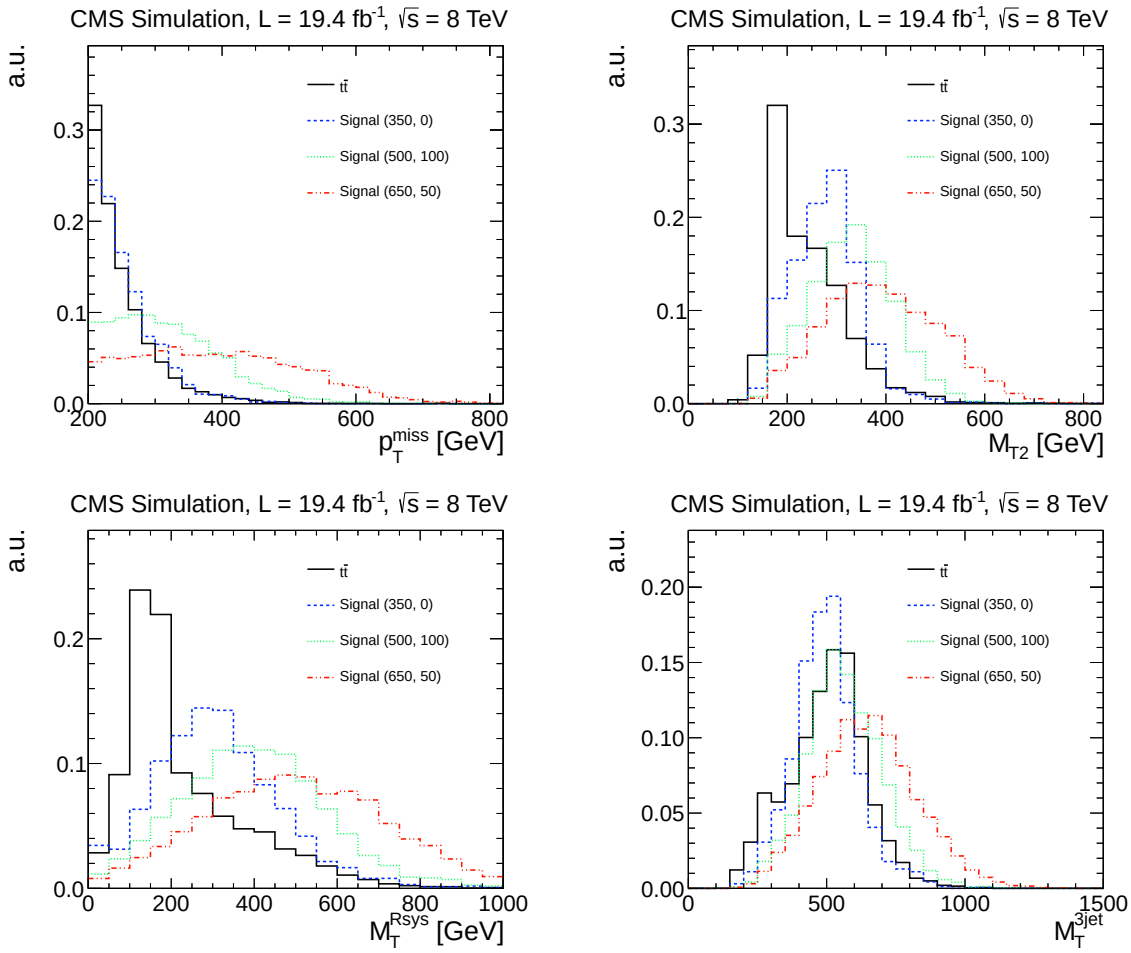

Figure 3: The $p_{\mathrm{T}}^{\mathrm{miss}}$, M_{T2}, $M_{\mathrm{T}}^{\text{3-jet}}$, and $M_{\mathrm{T}}^{\mathrm{Rsys}}$ distributions for $\mathrm{t\bar{t}}$ and three signal points after the pre-selection and a $p_{\mathrm{T}}^{\mathrm{miss}} > 200\,\mathrm{GeV}$ requirement. All distributions are normalized by the total number of events and the label "a.u." means arbitrary units. The signal points are labeled as "(X, Y)" where X is the top squark mass and Y is the $\tilde{\chi}_1^0$ mass.

tween $t\bar{t}$ and some signal points after the pre-selection and a $p_T^{miss} > 200\,GeV$ requirement. For signals with a $p_T^{miss} > 200\,GeV$ requirement, the two top quarks generally are in the opposite hemisphere as the $\vec{p}_T^{miss}$. Therefore the $\Delta\phi$ angles in both $M_T^{3\text{-jet}}$ and M_T^{Rsys} calculations are large which makes the two variables tend to have large values. For $t\bar{t}$ events with $p_T^{miss} > 200\,GeV$, the $\vec{p}_T^{miss}$ is close to either one of the two top quarks. Therefore a correlation between the M_T^{Rsys} and $M_T^{3\text{-jet}}$ can be used to reject this background.

Figure 4 shows 2D distributions of $M_T^{3\text{-jet}}$ versus M_T^{Rsys} for $t\bar{t}$ and some signal points for events passing the pre-selection and a $p_T^{miss} > 200\,GeV$ requirement. Based on simulation, a requirement on the linear combination of the $M_T^{3\text{-jet}}$ and M_T^{Rsys} variables gives better discriminating power than requirements on them separately. The full set of topological selections are:

- $M_{T2} \geq 300\,GeV$
- $(0.5 \cdot M_T^{3\text{-jet}} + M_T^{Rsys}) \geq 500\,GeV$.

The cuts on the event topological variables are optimized to reject as many $t\bar{t}$ events as possible while keeping good acceptances for a range of signal points.

Four search regions are defined by requiring $p_T^{miss} > 200\,GeV$ and $p_T^{miss} > 350\,GeV$ with at least 1 or at least 2 b-tagged jets. The requirement of $N_{b\text{-jets}} \geq 2$ increases the sensitivity for high mass top squark production. The search region with $p_T^{miss} > 200\,GeV$ and $N_{b\text{-jets}} \geq 1$ is also called the "baseline" search region in this analysis.

Comparisons of the p_T^{miss}, M_{T2}, and $0.5 \cdot M_T^{3\text{-jet}} + M_T^{Rsys}$ distributions among observed data, predicted backgrounds and two selective signal points are shown in Figure 5 for events passing the baseline selection requirements. The event yields in MC simulated samples, normalized to the data integrated luminosity, are also summarized in Table 1 after various requirements in the preselection and Table 2 for the four search regions described above, together with event yields observed in data. The background yields from MC simulated samples are shown separately for different processes. As shown in Table 1, the cuts on the topological variables from reconstructed top quarks suppress the dominant $t\bar{t}$ background by a factor of approximately 10^3 with typical signal efficiencies in the range 8–40%. The data and simulated background event yields show a good agreement; however, these simulated predictions are not used further in the search for main SM background processes. Instead, the contributions of the main SM background processes are estimated directly using SM-enriched samples from data for the robustness of the search. The respective methods are described in the following sections.

5 Standard model background estimation

SM backgrounds in this search arise mainly from $t\bar{t}$ and W + jets production when a W boson decays into a neutrino and a lepton. Events from these processes can pass the search criteria when an e or μ escapes detection or a τ decays hadronically. These backgrounds, as well as the contribution from QCD multijet production, are determined using the collider data as described in Sections 5.1, 5.2 and 5.4. The background arising from Z + jets production with the Z boson decaying into a pair of neutrinos is determined from simulated events that are scaled to match the data. Previous analyses used a data-driven method from the $Z(\mu\mu)$ + jets data to estimate the $Z(\nu\bar{\nu})$ + jets background [25–27]. The statistical uncertainty of this data-driven method with the specific requirements in this analysis is very large, so we instead use simulation for the nominal prediction. This procedure is discussed in Section 5.3. The SM backgrounds from other rare processes, such as $t\bar{t}Z$ production with $Z \to \nu\bar{\nu}$ or WZ and ZZ production with at

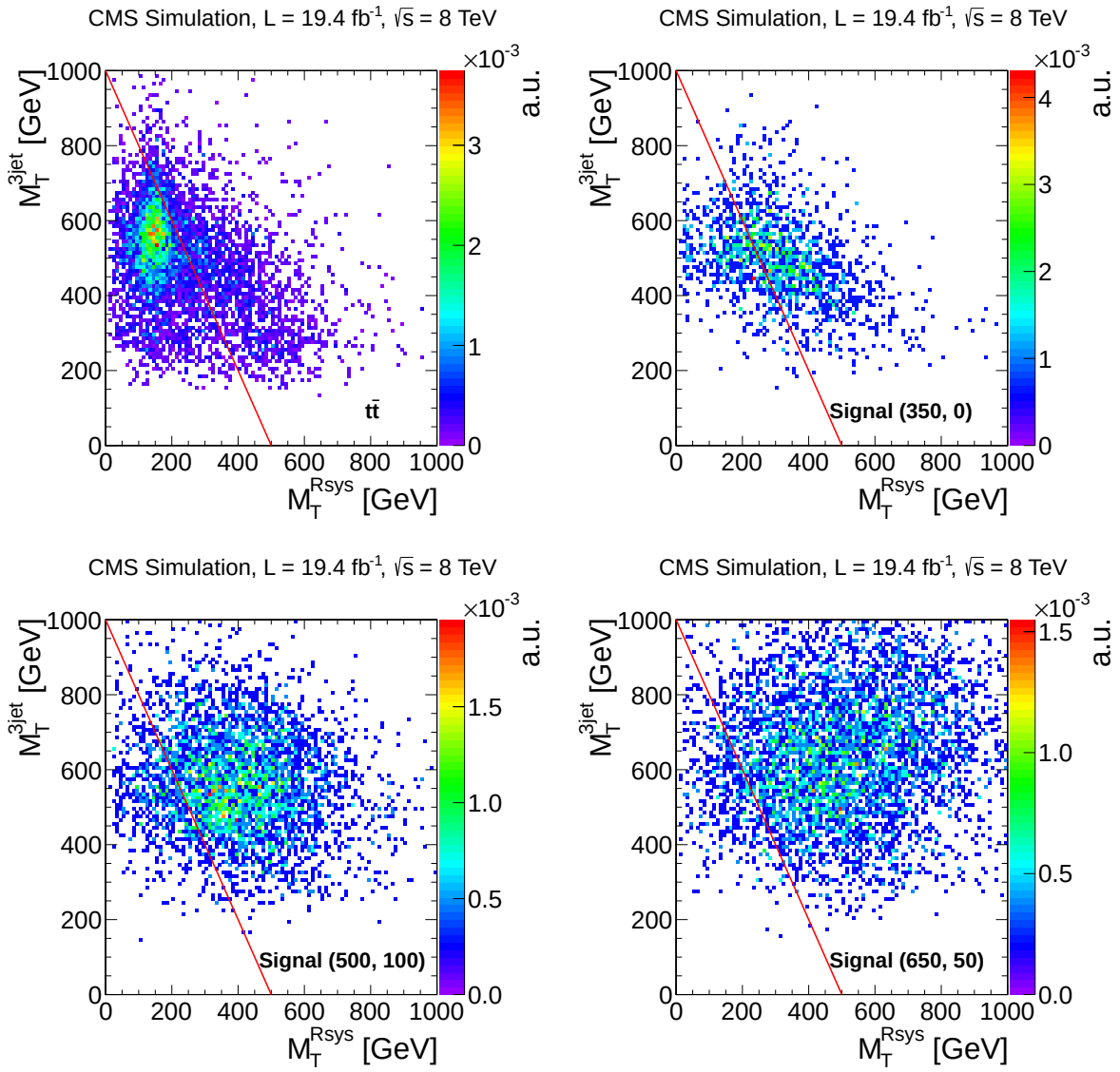

Figure 4: The 2D distributions of $M_{\mathrm{T}}^{\text{3-jet}}$ versus $M_{\mathrm{T}}^{\mathrm{Rsys}}$ for $\mathrm{t\bar{t}}$ and three signal points after the pre-selection and a $p_{\mathrm{T}}^{\mathrm{miss}} > 200\,\mathrm{GeV}$ requirement. All distributions are normalized by the total number of events and the label "a.u." means arbitrary units. The red line indicates the cut threshold. The signal points are labeled as "(X, Y)" where X is the top squark mass and Y is the $\tilde{\chi}_1^0$ mass.

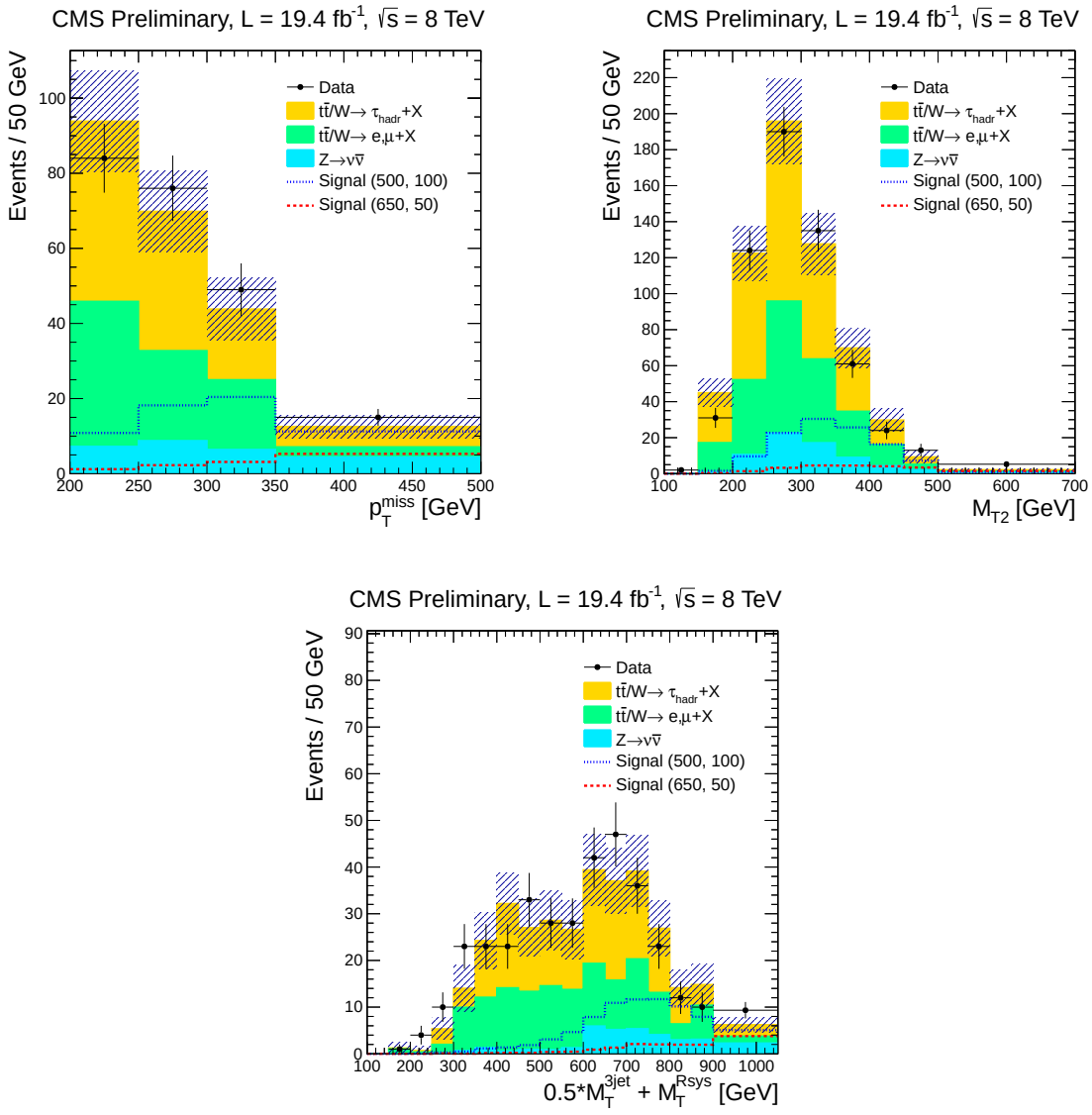

Figure 5: The $p_{\mathrm{T}}^{\mathrm{miss}}$, M_{T2}, and $0.5 \cdot M_{\mathrm{T}}^{\text{3-jet}} + M_{\mathrm{T}}^{\mathrm{Rsys}}$ distributions from observed data (black dots), predicted backgrounds (solid filled areas) and two selective signal points. The $p_{\mathrm{T}}^{\mathrm{miss}}$ distribution is obtained after applying the baseline selection cuts, while both the M_{T2} and the $0.5 \cdot M_{\mathrm{T}}^{\text{3-jet}} + M_{\mathrm{T}}^{\mathrm{Rsys}}$ distributions are obtained after baseline selection cuts without either the $M_{\mathrm{T2}} \geq 300\,\mathrm{GeV}$ or $0.5 \cdot M_{\mathrm{T}}^{\text{3-jet}} + M_{\mathrm{T}}^{\mathrm{Rsys}} \geq 500\,\mathrm{GeV}$ cut in order to show the relaxed control region for the two variables. The signal yields are scaled to 19.4 fb^{-1}. The QCD prediction is not included in the plots since its contribution is negligible. The dashed area indicates the total uncertainties including both statistical and systematic uncertainties for each bin. The last bin contains all the events above the maximum values of $p_{\mathrm{T}}^{\mathrm{miss}}$, M_{T2}, and $0.5 \cdot M_{\mathrm{T}}^{\text{3-jet}} + M_{\mathrm{T}}^{\mathrm{Rsys}}$ in the figures, respectively.

Table 1: Event yields and cut flow from MC simulated samples after various requirements in the preselection and kinematic cuts from the top quark reconstruction. All numbers are scaled to 19.4 fb^{-1}. Only statistical uncertainties are shown in the table. The signal points are labeled as "(X, Y)" where X is the top squark mass and Y is the $\tilde{\chi}_1^0$ mass. Data yields are omitted as the trigger is inefficient before the offline $p_{\mathrm{T}}^{\mathrm{miss}}$ cut at 200 GeV. The number of QCD multijet events is not included in the sum total as the QCD multijet background overwhelms all the other backgrounds in some columns which would render the sum total uninformative.

Process	e, μ vetos	jet counting	$\Delta\phi(\vec{p}_{\mathrm{T}}^{\mathrm{miss}}, \vec{p}_{\mathrm{T}}^{\mathrm{jet}})$	$N_{\text{b-jets}} \geq 1$	top reco. + kinematic cuts
$\mathrm{t\bar{t}}$	2652858 ± 746	626652 ± 363	364869 ± 277	314179 ± 257	229.7 ± 6.9
$\mathrm{W} \to \ell\nu$	1097574 ± 624	38143 ± 122	24594 ± 98	4767 ± 43	28.6 ± 3.2
$\mathrm{Z} \to \nu\bar{\nu}$	1053228 ± 425	9518 ± 27	6760 ± 23	1276 ± 10	28.2 ± 1.2
QCD	1955905397 ± 674400	85334931 ± 123627	48350298 ± 93847	9516527 ± 41181	116.4 ± 72.5
single top	1618682 ± 4685	51918 ± 623	29453 ± 468	24270 ± 433	24.4 ± 4.6
$\mathrm{t\bar{t}Z}$	2033 ± 6	1121 ± 5	676 ± 4	587 ± 3	9.3 ± 0.4
$\mathrm{t\bar{t}W}$	2088 ± 7	1096 ± 5	645 ± 4	548 ± 4	3.3 ± 0.3
ZZ	280826 ± 99	2203 ± 9	1239 ± 7	524 ± 4	0.9 ± 0.2
WZ	490185 ± 179	4086 ± 16	2312 ± 12	757 ± 7	0.7 ± 0.2
WW	728425 ± 287	5435 ± 25	3076 ± 19	768 ± 9	0.9 ± 0.3
Total (no QCD)	7925899 ± 4817	740177 ± 732	433625 ± 554	347676 ± 506	325.9 ± 9.1
Signal (350, 0)	8802 ± 53	3113 ± 31	2505 ± 28	2200 ± 26	182.9 ± 7.6
Signal (500, 100)	927 ± 6	419 ± 4	360 ± 3	314 ± 3	85.9 ± 1.7
Signal (650, 50)	152 ± 1	75 ± 1	66 ± 1	58 ± 1	22.7 ± 0.4

least one vector boson decaying into a neutrino, are estimated directly from the MC simulated samples and are found to be rather small, as described in Section 4.

5.1 Hadronic decay of τ leptons produced in W boson decay

The hadronic decay of τ leptons (τ_{h}) is the largest component of the background estimate from W + jets or $\mathrm{t\bar{t}}$ events in the search regions. The presence of neutrinos in the final state results in $\vec{p}_{\mathrm{T}}^{\mathrm{miss}}$, and the event passes the lepton veto because the hadronically decaying τ is reconstructed as a jet. This background is estimated from a data sample of μ + jets events selected from $\mu + \geq$3-jet triggers by requiring exactly one μ with $p_{\mathrm{T}}^{\mu} > 20\,\mathrm{GeV}$ and $|\eta| < 2.1$. The transverse mass of the W boson $m_{\mathrm{T}} = \sqrt{2p_{\mathrm{T}}^{\mu} p_{\mathrm{T}}^{\mathrm{miss}}(1 - \cos\Delta\phi)}$ is required to be less than 100 GeV in order to select events containing a $\mathrm{W} \to \mu\nu$ decay and to suppress possible new physics signal contamination, i.e., the signal events included in the μ + jets sample. Here, $\Delta\phi$ is the azimuthal angle between the $\vec{p}_{\mathrm{T}}{}^{\mu}$ and the $\vec{p}_{\mathrm{T}}^{\mathrm{miss}}$ directions. Because the μ + jets and τ_{h} + jets events arise from the same physics processes, the hadronic component of the two samples is the same except for the response of the detector to the muon or τ_{h} jet. To account for this difference, the muon in data is replaced by a simulated τ_{h} jet with the p_{T} sampled randomly from a response function for a hadronically-decaying τ lepton. The N_{jets}, $\vec{p}_{\mathrm{T}}^{\mathrm{miss}}$, M_{T2}, $M_{\mathrm{T}}^{\text{3-jet}}$ and $M_{\mathrm{T}}^{\mathrm{Rsys}}$ of the event are recalculated with this τ_{h} jet, and the search selections are applied to predict the τ_{h} background. The τ_{h}-jet response function $p_{\mathrm{T}}^{\mathrm{jet}} / p_{\mathrm{T}}^{\tau}$ is obtained from simulated $\mathrm{t\bar{t}}$ events, in which the tau-lepton decays were handled with TAUOLA 27.121.5 [62], by matching the reconstructed τ jet with the generated τ lepton decaying hadronically, in the bins of the originating τ momentum. In order to sample the complete response template, this procedure is repeated multiple times for each event. Corrections are applied to account for the trigger efficiency, acceptance and efficiency of the μ selection, m_{T} cut efficiency, contamination from the $\tau \to \mu$ decays and the ratio of branching fractions $\mathcal{B}(\mathrm{W} \to \tau_{\mathrm{h}}\nu)/\mathcal{B}(\mathrm{W} \to \mu\nu) = 0.65$ [63]. The predicted τ_{h} background and uncertainties are shown in Table 3 for all the search regions.

Table 2: Event yields and cut flow from MC simulated samples continued from Table 1 for the four signal regions, and the observed yields in data. All numbers are scaled to 19.4 fb^{-1}. Only statistical uncertainties are shown in the table. The signal points are labeled as "(X, Y)" where X is the top squark mass and Y is the $\tilde{\chi}_1^0$ mass. The number of QCD multijet events is not included in the sum total as the QCD multijet background is negligible in all four signal regions.

	$p_T^{miss} > 200$ GeV, $N_{b\text{-jets}} \geq 1$	$p_T^{miss} > 350$ GeV, $N_{b\text{-jets}} \geq 1$	$p_T^{miss} > 200$ GeV, $N_{b\text{-jets}} \geq 2$	$p_T^{miss} > 350$ GeV, $N_{b\text{-jets}} \geq 2$
$t\bar{t}$	153.8 ± 5.7	18.9 ± 2.0	63.4 ± 3.7	6.3 ± 1.2
$W \to \ell\nu$	22.9 ± 2.9	5.8 ± 1.4	3.9 ± 1.2	1.1 ± 0.6
$Z \to \nu\bar{\nu}$	25.0 ± 1.2	8.4 ± 0.6	4.6 ± 0.5	1.3 ± 0.2
QCD	1.1 ± 0.6	$0.0^{+0.5}_{-0.0}$	$0.0^{+0.5}_{-0.0}$	$0.0^{+0.5}_{-0.0}$
single top	17.5 ± 3.9	5.2 ± 2.1	7.0 ± 2.5	1.8 ± 1.2
$t\bar{t}Z$	7.8 ± 0.4	2.3 ± 0.2	4.2 ± 0.3	1.4 ± 0.2
$t\bar{t}W$	2.4 ± 0.2	0.3 ± 0.1	1.1 ± 0.2	0.1 ± 0.1
ZZ	0.8 ± 0.2	0.3 ± 0.1	0.2 ± 0.1	$0.0^{+0.1}_{-0.0}$
WZ	0.5 ± 0.2	0.1 ± 0.1	0.1 ± 0.1	$0.0^{+0.1}_{-0.0}$
WW	0.8 ± 0.3	0.1 ± 0.1	0.3 ± 0.2	$0.0^{+0.2}_{-0.0}$
Total (no QCD)	231.5 ± 7.6	41.2 ± 3.3	84.7 ± 4.6	12.0 ± 1.8
Data	254	45	83	15
Signal (350, 0)	162.8 ± 7.2	11.3 ± 1.9	84.4 ± 5.2	7.5 ± 1.5
Signal (500, 100)	83.2 ± 1.7	33.7 ± 1.1	48.1 ± 1.3	19.8 ± 0.8
Signal (650, 50)	22.4 ± 0.4	15.8 ± 0.3	13.1 ± 0.3	9.3 ± 0.2

The τ_h background estimation method is validated by applying it to the $t\bar{t}$ and W + jets MC samples. A comparison of predicted distributions of p_T^{miss} and M_{T2} with true τ_h background events is shown in Fig. 6 for the baseline selection. For the p_T^{miss} and M_{T2} variables, the predicted distributions reproduce the expected distributions within statistical uncertainties.

Due to the multiple sampling of the response template, the statistical uncertainty on the prediction is evaluated with a set of pseudo-experiments using a bootstrap technique [64]. The main systematic uncertainties in the hadronic-τ background estimation arise from the statistical power of the validation to this method (6–21%), the μ acceptance (3–4%) and the τ-jet response function (2–3%) [65]. An additional uncertainty of (3–14%) is assigned on the predicted events to account for possible differences between data and MC on the acceptance of the m_T selection. Since the uncertainty is different for each search region, only the ranges are quoted above.

Table 3: Predicted hadronic tau background corresponding to 19.4 fb^{-1} from the methods here presented in all four search regions.

Region	Prediction
$p_T^{miss} > 200$ GeV, $N_{b\text{-jets}} \geq 1$	120.2 ± 7.4 (stat) $^{+9.3}_{-9.3}$ (syst)
$p_T^{miss} > 350$ GeV, $N_{b\text{-jets}} \geq 1$	16.5 ± 2.1 (stat) $^{+2.7}_{-2.7}$ (syst)
$p_T^{miss} > 200$ GeV, $N_{b\text{-jets}} \geq 2$	45.3 ± 4.3 (stat) $^{+5.5}_{-5.5}$ (syst)
$p_T^{miss} > 350$ GeV, $N_{b\text{-jets}} \geq 2$	4.3 ± 1.4 (stat) $^{+1.0}_{-1.1}$ (syst)

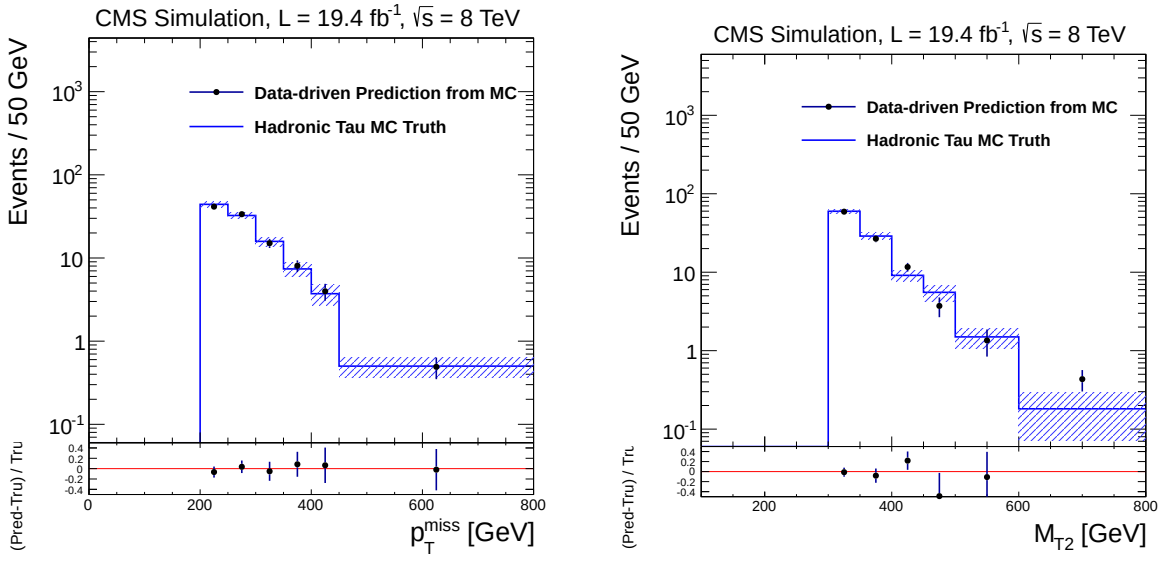

Figure 6: Comparison of predicted distributions of $p_{\mathrm{T}}^{\mathrm{miss}}$ (left) and M_{T2} (right) with the truth in MC simulated $\mathrm{t\bar{t}}$ and W + jets events containing a hadronically decaying τ lepton. Only the statistical uncertainties are shown on the predicted distributions.

5.2 Lost leptons from a W boson decaying to an electron or muon

The $\mathrm{W}(\ell\nu)$ + jets events (ℓ = e or μ) from $\mathrm{t\bar{t}}$ and W + jets production constitute a background when an electron or muon is not identified (~60% of the lost lepton background), not isolated (~10%), or is out of the detector acceptance (~30%), and therefore escapes the lepton veto described in Section 4. Such leptons are referred to as "lost leptons". Events with lost electrons or muons from leptonically decaying taus are also taken into account. This background is estimated from a μ + jets control sample selected with the same criteria as those used for the search except that we require an event to have exactly one well reconstructed μ with p_{T}^{μ} >5 GeV. As in the estimation of the hadronically-decaying τ leptons background, only the events with $m_{\mathrm{T}} < 100$ GeV are considered.

Using the reconstruction and isolation efficiencies, $\epsilon_{\mathrm{reco}}^{\mathrm{e},\mu}$ and $\epsilon_{\mathrm{iso}}^{\mathrm{e},\mu}$, respectively, of the electrons and muons, the events in the isolated muon control sample are weighted according to

- $\left(1/\epsilon_{\mathrm{iso}}^{\mu}\right)\left[(1-\epsilon_{\mathrm{reco}}^{\mathrm{e},\mu})/\epsilon_{\mathrm{reco}}^{\mu}\right]$ to predict events with unidentified leptons and
- $\left(\epsilon_{\mathrm{reco}}^{\mathrm{e},\mu}/\epsilon_{\mathrm{reco}}^{\mu}\right)\left[(1-\epsilon_{\mathrm{iso}}^{\mathrm{e},\mu})/\epsilon_{\mathrm{iso}}^{\mu}\right]$ to estimate events with nonisolated leptons in the signal region.

The lepton isolation and reconstruction efficiencies and kinematic acceptance are obtained from MC simulation of $\mathrm{t\bar{t}}$ events and are determined in lepton p_{T} bins after our baseline cuts. They are validated with tag-and-probe studies of Z→ll events in data and MC simulation.

This estimation method, based on the collision data, is validated by predicting the lost lepton background using a single muon sample from simulated $\mathrm{t\bar{t}}$ and W + jets events and comparing the predicted and the expected true distributions. Comparisons of the predicted and the expected distributions of $p_{\mathrm{T}}^{\mathrm{miss}}$ and M_{T2} for events with a lost-lepton in the baseline selection region are shown in Figure 7. The predicted distributions closely reproduce the expected dis-

tribution of sensitive variables used for this search.

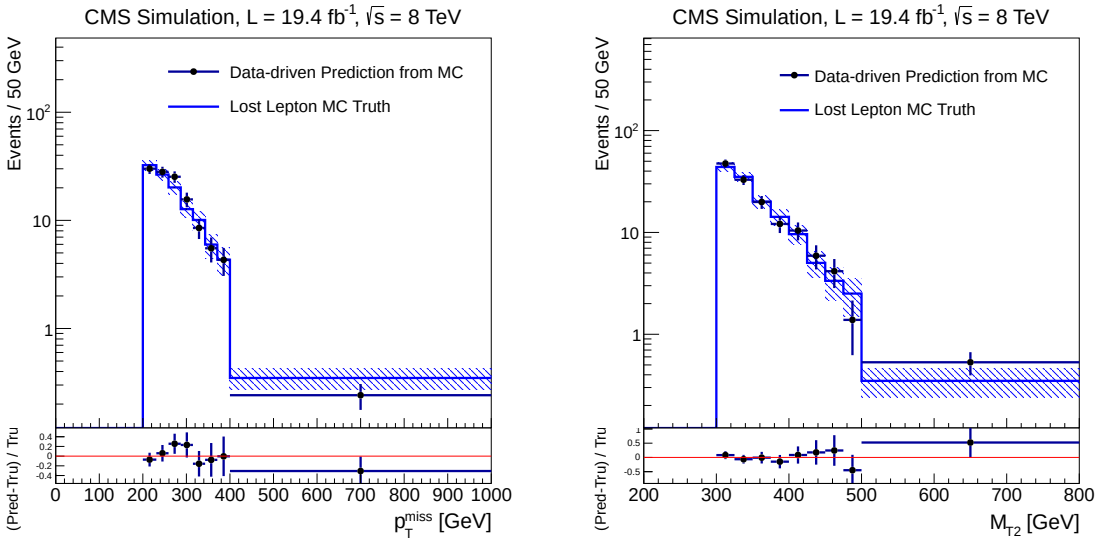

Figure 7: Predicted distributions of $p_{\mathrm{T}}^{\mathrm{miss}}$ (left) and M_{T2} (right) compared to the truth in the $\mathrm{t\bar{t}}$ and W + jets MC simulated events containing an undetected lepton (e or μ).

The prediction is obtained by applying this method to the μ + jets sample collected using the same jets + $p_{\mathrm{T}}^{\mathrm{miss}}$ trigger which is used to collect the signal events. The predicted lost-lepton events and uncertainties for each search region are listed in Table 4. The dominant uncertainties on the lost-lepton prediction arise from the difference in lepton reconstruction and isolation efficiencies between data and MC. In order to account for possible differences in lepton reconstruction efficiencies in data and MC, these efficiencies are estimated by applying a "tag and probe" method [66] on $\mathrm{Z} \to \mu^+\mu^-$ events in data and simulation. For isolation uncertainties, the MC isolation variables are scaled to match the data distribution and the resulting differences in predictions are taken as systematic uncertainties for the data and MC differences. The variations of the parton density functions following the recommendation of Ref. [67] change the muon acceptance and leads to less than 3.3% uncertainty on the final prediction. An additional uncertainty of 3% is assigned to account for possible difference in data and MC on the acceptance of m_{T} selection and is mostly expected to arise from $p_{\mathrm{T}}^{\mathrm{miss}}$ tail.

Table 4: Lost lepton prediction results for $19.4\,\mathrm{fb}^{-1}$.

Region	Prediction
$p_{\mathrm{T}}^{\mathrm{miss}} > 200\,\mathrm{GeV}$, $N_{\text{b-jets}} \geq 1$	$89.3 \pm 8.4\ (\text{stat})\ ^{+20.2}_{-19.2}\ (\text{syst})$
$p_{\mathrm{T}}^{\mathrm{miss}} > 350\,\mathrm{GeV}$, $N_{\text{b-jets}} \geq 1$	$8.2 \pm 2.6\ (\text{stat})\ ^{+3.0}_{-3.0}\ (\text{syst})$
$p_{\mathrm{T}}^{\mathrm{miss}} > 200\,\mathrm{GeV}$, $N_{\text{b-jets}} \geq 2$	$33.8 \pm 5.2\ (\text{stat})\ ^{+8.9}_{-8.5}\ (\text{syst})$
$p_{\mathrm{T}}^{\mathrm{miss}} > 350\,\mathrm{GeV}$, $N_{\text{b-jets}} \geq 2$	$1.2 \pm 0.8\ (\text{stat})\ ^{+0.6}_{-0.6}\ (\text{syst})$

5.3 Z boson decaying into neutrinos

Z + jets production contributes a background in this search when the Z boson decays to neutrinos ($\mathrm{Z}(\nu\bar{\nu})$). This background is estimated by applying a scale factor to simulated events to match the data. The simulation is validated using $\mathrm{Z}(\mu\mu)$ + jets events, and then a prediction

is derived from $Z(\nu\bar{\nu})$ + jets simulation. The background cannot be estimated directly from the data because very few $Z(\mu\mu)$ + jets data events survive the selection criteria, specifically the top-tagging requirements. This leads to poor data statistics and an extreme quantization of the estimate. Instead, the fully data-based method is used internally as a cross check to the method described here. The scaling factor $R^{\mu\mu}_{\text{data/MC}}$ is the ratio of the $Z(\mu\mu)$ + jets event rate measured in the data to the rate predicted by simulation. These rates are measured by selecting events that satisfy the pre-selection criteria of Section 4.2 with the exception that the lepton veto is replaced by the requirement of a dimuon pair with a pair mass in the range 71–111 GeV and the muons are treated as neutrinos and added into the $\vec{p}_{\text{T}}^{\text{miss}}$.

The scaling factor is found to be 1.36 ± 0.17 (stat). This factor is also estimated to be 1.40 ± 0.50 (stat) using the subset of events with 2 or more b-tagged jets. These scale factors are due to an observed under-estimation of Z bosons accompanied by reconstructed b-tagged jets in the simulation. The scale factor for events with exactly 0 b-tagged jet is statistically consistent with 1.

In data, the di-muon events passing the above requirements include contributions from $\mathrm{t\bar{t}}$ and $\mathrm{t\bar{t}Z}$ events. The $\mathrm{t\bar{t}}$ contribution is estimated using the yield of simulated $\mathrm{t\bar{t}}$ events scaled for the measured differences between MC and data. The data-MC scale factor is estimated from events with a reconstructed muon with $p_{\text{T}} > 20\,\text{GeV}$, an electron with $p_{\text{T}} > 20\,\text{GeV}$, the five highest p_{T} jets passing the signal selection requirements, and at least one b-tagged jet. The scale factor is measured to be 1.00 ± 0.06 (stat). The small $\mathrm{t\bar{t}Z}$ contribution is estimated directly from simulation.

To determine the contribution in the search regions, the $Z(\nu\bar{\nu})$ yields passing all the requirements are determined from the simulation and multiplied by $R^{\mu\mu}_{\text{data/MC}}$.

The uncertainty on the $Z(\nu\bar{\nu})$ prediction is dominated by the statistical uncertainty in the tails of the kinematic selection variables that are used to extrapolate the normalization from the loose requirements defined above to the search regions. Three main effects are considered: uncertainties on the measurement of the normalization factor, which include both the statistical uncertainties both on the data and simulation and the extrapolation of the measurement into the signal regions, the uncertainties from the subtraction of $\mathrm{t\bar{t}}$ and $\mathrm{t\bar{t}Z}$ events, and the uncertainty on the acceptance differences between $Z(\nu\bar{\nu})$ and $Z(\mu\mu)$ events. The uncertainty in the extrapolation is estimated by studying the ratio between data and simulation of the $p_{\text{T}}^{\text{miss}}$, $\Delta\phi$, M_{T2}, $M_{\text{T}}^{\text{3-jet}}$ and $M_{\text{T}}^{\text{Rsys}}$ distributions. It is assumed that differences between simulation and data are at worst linear in the relevant variable, so each ratio is fit with a first order polynomial function. For each distribution, the uncertainty envelope of the fit is estimated at the average value of the variable for all events surviving the corresponding selection requirement. When this uncertainty envelope extends above or below the statistical uncertainty measured in the normalization region, a residual asymmetrical uncertainty is assigned equal to the difference between the two windows. This uncertainty is summed in quadrature across the considered distributions. In the case of the ≥ 2 b-tagged jet selection, the fit uncertainty is very large due to low data statistics. This causes the residual uncertainty to dominate in this search region.

The $Z(\nu\bar{\nu})$ predictions for the four search regions along with total systematic uncertainties are given in Table 5.

An alternative method to predict the $Z(\nu\bar{\nu})$ is to scale the number of observed $Z(\mu\mu)$ events in the data by the simulation predicted ratio between $Z(\nu\bar{\nu})$ and $Z(\mu\mu)$ production, accounting for the differences in acceptance, efficiency, and the $Z(\mu\mu)$ and $Z(\nu\bar{\nu})$ branching fractions. However, very few $Z(\mu\mu)$ events pass all the selection criteria, and the difference of one event

Table 5: Prediction for the Z to invisible background for the various signal regions.

Region	Prediction
$p_T^{miss} > 200\,GeV$, $N_{b\text{-jets}} \geq 1$	35.8 ± 1.9 (stat) $^{+16.2}_{-18.9}$ (syst)
$p_T^{miss} > 350\,GeV$, $N_{b\text{-jets}} \geq 1$	13.2 ± 1.1 (stat) $^{+6.4}_{-7.8}$ (syst)
$p_T^{miss} > 200\,GeV$, $N_{b\text{-jets}} \geq 2$	6.1 ± 0.7 (stat) $^{+15.3}_{-5.5}$ (syst)
$p_T^{miss} > 350\,GeV$, $N_{b\text{-jets}} \geq 2$	1.8 ± 0.4 (stat) $^{+6.8}_{-1.6}$ (syst)

can change the prediction by up to 30 events. Since this method suffers from such quantization effects, it is used only to cross check the above predictions. The results from this method agree with the predictions given in Table 5 within the uncertainties.

5.4 QCD multijet production

Due to the p_T^{miss} and $\Delta\phi$ requirements, the QCD multijet background contribution in the search region is nearly negligible. An estimate of this contribution is made by measuring the number of QCD multijet events in a control region and scaling this number by a translation factor R_{QCD}. The control region is identical to the search region except that the $\Delta\phi$ requirement is inverted: one of the three highest p_T jets must fail the requirement that the azimuthal angle between $\vec{p}_T$ and the p_T^{miss} vector, $\Delta\phi(j, \text{miss})$, is larger than 0.5, 0.5, and 0.3 radians, respectively. R_{QCD} is the ratio between the number of QCD multijet events in the search region and that in the inverted $\Delta\phi$ region.

Since the selection requires one reconstructed top quark, at least one b-tagged jet, and large p_T^{miss}, the control regions are dominated by $t\bar{t}$, $Z(\nu\bar{\nu})$, and W + jet events. Thus, in order to estimate the number of QCD multijet events in the control regions, the number of events in data are corrected for the non-QCD multijet contributions using the same background prediction methods mentioned in the previous sections.

The scale factor R_{QCD} is first found in a $175 < p_T^{miss} < 200\,GeV$ sideband by measuring the number of QCD multijet events both with the standard and inverted $\Delta\phi$ requirements. Then, using simulated events, R_{QCD} is measured as a function of p_T^{miss} and fit with a first order polynomial. The slope of this polynomial is used to extrapolate the R_{QCD} value measured in the $175 < p_T^{miss} < 200\,GeV$ control region to the higher p_T^{miss} search regions. The MC statistical uncertainty, jet energy scale uncertainty, and jet energy resolution uncertainty all contribute to the systematic uncertainty on the scale factor.

The QCD multijet background prediction is given in Table 6 for each of the four search regions. The systematic uncertainties arise from uncertainties on R_{QCD} and the non-QCD multijet subtraction.

Table 6: QCD multijet prediction for each of the four search regions.

Region	QCD, inverted $\Delta\phi$	Predicted R_{QCD}	Final QCD Prediction
$p_T^{miss} > 200\,GeV$, $N_{b\text{-jets}} \geq 1$	70.2 ± 12.6 (stat) ± 13.8 (syst)	$0.04^{+0.25}_{-0.04}$ (syst)	3.2 ± 0.6 (stat) $^{+18.2}_{-3.2}$ (syst)
$p_T^{miss} > 350\,GeV$, $N_{b\text{-jets}} \geq 1$	6.6 ± 3.7 (stat) ± 1.9 (syst)	$0.15^{+0.29}_{-0.15}$ (syst)	1.0 ± 0.5 (stat) $^{+1.9}_{-1.0}$ (syst)
$p_T^{miss} > 200\,GeV$, $N_{b\text{-jets}} \geq 2$	$1.1^{+6.2}_{-1.1}$ (stat) $^{+6.7}_{-1.1}$ (syst)	$0.05^{+0.40}_{-0.05}$ (syst)	$0.05^{+0.30}_{-0.05}$ (stat) $^{+0.55}_{-0.05}$ (syst)
$p_T^{miss} > 350\,GeV$, $N_{b\text{-jets}} \geq 2$	$0.7^{+2.0}_{-0.7}$ (stat) $^{+1.4}_{-0.7}$ (syst)	$0.14^{+0.41}_{-0.14}$ (syst)	$0.10^{+0.28}_{-0.10}$ (stat) $^{+0.35}_{-0.10}$ (syst)

6 Results

The predicted number of SM events and the number of events observed in data in each of the four search regions defined in Section 4 are summarized in Table 7. The most significant background in all search regions comes from the SM $\mathrm{t\bar{t}}$ production. For the baseline selection, 35% comes from $\mathrm{W}(\mu\nu)$ and $\mathrm{W}(e\nu)$ decays where the electron or muon from W decays are not detected and 47% from $\mathrm{W}(\tau\nu)$ where the τ lepton decays hadronically. The next largest contribution comes from $Z(\nu\nu)$ + jet production in which a pair of neutrinos gives large $p_{\mathrm{T}}^{\mathrm{miss}}$ and the top quark conditions are satisfied by an accidental combination of the jets. Among other rare processes considered, the dominant contribution comes from $\mathrm{t\bar{t}Z}$ with the Z boson decaying into a pair of neutrinos. This background is determined from the simulation with an associated systematic uncertainty of 50%. The QCD multijet contribution is negligible.

Table 7: Predicted event yields from the different background estimation methods for the search regions defined in Section 4. The uncertainties on various backgrounds are added in quadrature for the uncertainty on the total background estimation.

Search region	$\mathrm{Z} \to \nu\bar{\nu}$	$\mathrm{t\bar{t}}/\mathrm{W} \to \mathrm{e}, \mu + \mathrm{X}$	$\mathrm{t\bar{t}}/\mathrm{W} \to \tau_{\mathrm{h}} + \mathrm{X}$	QCD	Rare processes	Total background	Obs. data
$p_{\mathrm{T}}^{\mathrm{miss}} > 200\,\mathrm{GeV}$, $N_{\text{b-jets}} \geq 1$	$35.8\,^{+16.3}_{-19.0}$	$89.3\,^{+21.9}_{-21.0}$	$120.2\,^{+11.8}_{-11.9}$	$3.2\,^{+18.2}_{-3.2}$	$5.8\,^{+2.9}_{-2.9}$	$254.3\,^{+35.0}_{-31.0}$	254
$p_{\mathrm{T}}^{\mathrm{miss}} > 350\,\mathrm{GeV}$, $N_{\text{b-jets}} \geq 1$	$13.2\,^{+6.5}_{-7.9}$	$8.2\,^{+4.0}_{-4.0}$	$16.5\,^{+3.4}_{-3.4}$	$1.0\,^{+1.9}_{-1.0}$	$2.0\,^{+1.0}_{-1.0}$	$40.9\,^{+8.6}_{-9.6}$	45
$p_{\mathrm{T}}^{\mathrm{miss}} > 200\,\mathrm{GeV}$, $N_{\text{b-jets}} \geq 2$	$6.1\,^{+15.3}_{-5.5}$	$33.8\,^{+10.3}_{-10.0}$	$45.3\,^{+7.0}_{-7.0}$	$0.1\,^{+0.6}_{-0.1}$	$3.1\,^{+1.6}_{-1.6}$	$88.4\,^{+19.8}_{-13.5}$	83
$p_{\mathrm{T}}^{\mathrm{miss}} > 350\,\mathrm{GeV}$, $N_{\text{b-jets}} \geq 2$	$1.8\,^{+6.8}_{-1.6}$	$1.2\,^{+1.0}_{-1.0}$	$4.3\,^{+1.7}_{-1.8}$	$0.1\,^{+0.5}_{-0.1}$	$1.2\,^{+0.6}_{-0.6}$	$8.6\,^{+7.1}_{-2.7}$	15

7 Interpretation

The observed data yields are consistent with SM expectations. A modified frequentist CLs method is used taking a profile likelihood as a test statistic [68–70] in order to determine the upper limit on the possible contributions from non-SM processes in this search. In particular, these results are used to set limits on the signal model of scalar top quark pair production. The cross sections are determined at the NLO in the strong coupling constant and include the resummation of soft gluon emission at the accuracy of next-to-leading-log (NLL) level [71–76].

The uncertainties on the background predictions, the luminosity determination (2.6%) [24], the signal acceptance and efficiency arising from the jet energy correction and jet energy resolution (5%) [36], parton distribution functions (PDF) of the proton [67], trigger inefficiency (2%), the event cleaning procedure (3%) [58, 59], the uncertainties related to the initial/final state radiation (ISR/FSR) (1–23%) [19], and b-tagging data/MC scale factors (2–25%) [37] are all taken into account when the limits are determined. Potential contributions of signal events that result in the data samples used for the background estimations are less than 3% of the signal yields in the region relevant to this search and the effects on the limits are negligible. The acceptance of the signal is obtained after re-weighting the signal events with both the b-tagging scale factors and corrections of the initial state radiation in signal MC generation to match that measured in data [19].

As the four search regions are not mutually exclusive, one of the four search regions is selected at each point in the signal topology scan based on the best expected upper limit for providing the resulting cross section upper limit. The observed cross section upper limits on the signal model considered are shown in Figure 8, together with the two curves that correspond to points for which the observed and expected upper limits equal the theoretical signal cross sections.

The observed exclusion curves are also shown for the cases in which the signal cross section is varied by changing the renormalization and factorization scales by a factor of 2 and using the PDF4LHC recommendation [67] for the PDF uncertainty to illustrate the sensitivity of the exclusion to the signal cross section uncertainty. For small $\tilde{\chi}_1^0$ masses, our median expected limit reaches 620 GeV of top squark mass and our observed limit excludes top squark masses below 535 GeV at 95% confidence-level when the signal cross section minus its theoretical uncertainty is conservatively considered.

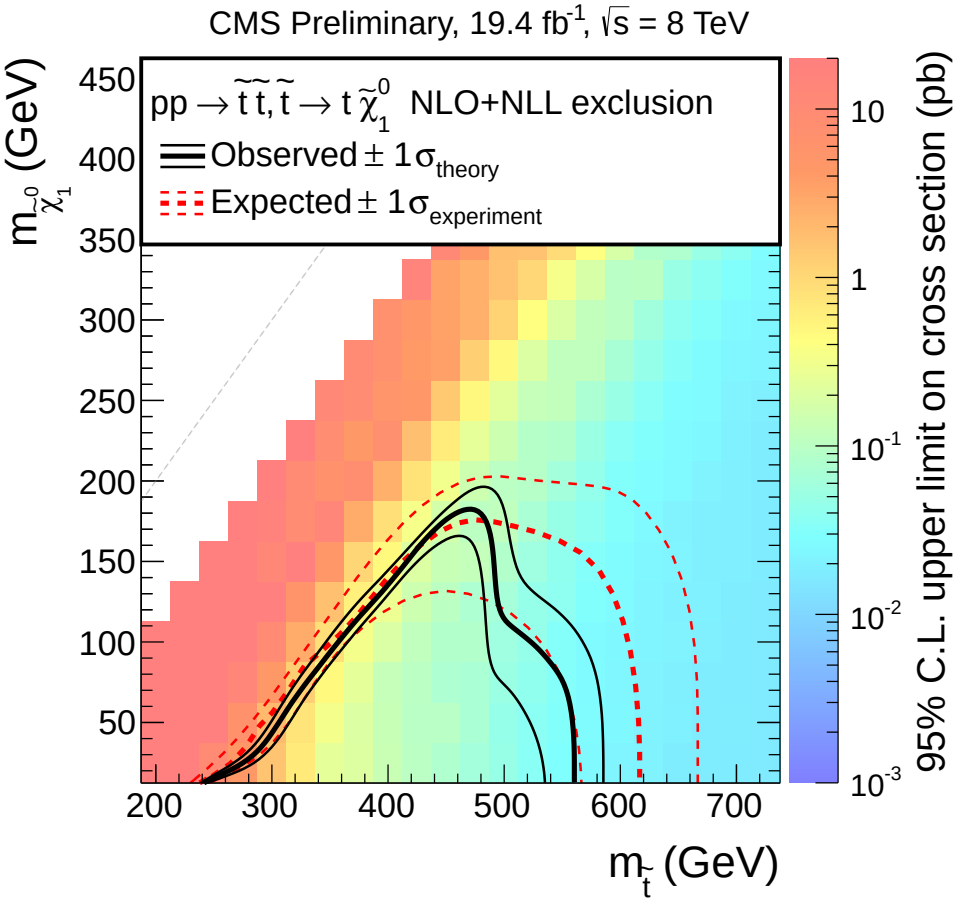

Figure 8: Combined 95% C.L. exclusion limits for the top squark pair production (signal topology). The plot shows the expected limit in red dashed line. The observed limit is shown in black solid line. The thinner dashed lines around the expected limit shows the variation in the expected limit, while the thinner solid curves show the variation in the observed limit when the signal cross section is varied by its theoretical uncertainties.

8 Conclusions

In summary, a search has been performed in events with two tops and large $p_{\mathrm{T}}^{\mathrm{miss}}$ signature using a data sample corresponding to an integrated luminosity of 19.4 fb^{-1} collected in 8 TeV pp collisions during the year 2012 with the CMS detector at the LHC. The observed number of events are consistent with the SM background contributions estimated from data. The results are presented in the context of a top-squark pair production model in which top squarks decaying to a top quark and a stable weakly interacting stable neutral particle $\tilde{\chi}_1^0$. For $\tilde{\chi}_1^0$ masses

less than 10 GeV, top squark masses below 535 GeV are excluded at 95% confidence-level.

References

[1] CMS Collaboration, "Observation of a new boson at a mass of 125 GeV with the CMS experiment at the LHC", *Phys. Lett. B* **716** (2012) 30, doi:10.1016/j.physletb.2012.08.021, arXiv:1207.7235.

[2] ATLAS Collaboration, "Observation of a new particle in the search for the Standard Model Higgs boson with the ATLAS detector at the LHC", *Phys. Lett. B* **716** (2012) 1, doi:10.1016/j.physletb.2012.08.020, arXiv:1207.7214.

[3] S. Dimopoulos and S. Raby, "Supercolor", *Nucl. Phys. B* **192** (1981) 353, doi:10.1016/0550-3213(81)90430-2.

[4] E. Witten, "Dynamical Breaking of Supersymmetry", *Nucl. Phys. B* **188** (1981) 513, doi:10.1016/0550-3213(81)90006-7.

[5] M. Dine, W. Fischler, and M. Srednicki, "Supersymmetric Technicolor", *Nucl. Phys. B* **189** (1981) 575, doi:10.1016/0550-3213(81)90582-4.

[6] S. Dimopoulos and H. Georgi, "Softly Broken Supersymmetry and SU(5)", *Nucl. Phys. B* **193** (1981) 150, doi:10.1016/0550-3213(81)90522-8.

[7] N. Sakai, "Naturalness in supersymmetric GUTS", *Z. Phys. C* **11** (1981) 153, doi:10.1007/BF01573998.

[8] R. K. Kaul and P. Majumdar, "Cancellation of quadratically divergent mass corrections in globally supersymmetric spontaneously broken gauge theories", *Nucl. Phys. B* **199** (1982) 36, doi:10.1016/0550-3213(82)90565-X.

[9] R. Barbieri and G. Giudice, "Upper bounds on supersymmetric particle masses", *Nucl. Phys. B* **306** (1988) 63, doi:10.1016/0550-3213(88)90171-X.

[10] B. de Carlos and J. Casas, "One-loop analysis of the electroweak breaking in supersymmetric models and the fine-tuning problem", *Phys. Lett. B* **309** (1993) 320, doi:10.1016/0370-2693(93)90940-J.

[11] S. Dimopoulos and G. Giudice, "Naturalness constraints in supersymmetric theories with non-universal soft terms", *Phys. Lett. B* **357** (1995) 573, doi:10.1016/0370-2693(95)00961-J.

[12] R. Barbieri, G. Dvali, and L. J. Hall, "Predictions from a U(2) flavour symmetry in supersymmetric theories", *Phys. Lett. B* **377** (1996) 76, doi:10.1016/0370-2693(96)00318-8.

[13] M. Papucci, J. T. Ruderman, and A. Weiler, "Natural SUSY endures", *JHEP* **1209** (2012) 035, doi:10.1007/JHEP09(2012)035, arXiv:1110.6926.

[14] V. Trimble, "Existence and Nature of Dark Matter in the Universe", *Ann. Rev. Astron. Astrophys.* **25** (1987) doi:10.1146/annurev.aa.25.090187.002233.

[15] J. L. Feng, "Dark Matter Candidates from Particle Physics and Methods of Detection", *Ann. Rev. Astron. Astrophys.* **48** (2010) doi:10.1146/annurev-astro-082708-101659, arXiv:1003.0904.

[16] ATLAS Collaboration, "Search for a supersymmetric partner to the top quark in final states with jets and missing transverse momentum at $\sqrt{s}$ = 7 TeV with the ATLAS detector", *Phys. Rev. Lett.* **109** (2012) 211802, doi:10.1103/PhysRevLett.109.211802, arXiv:1208.1447.

[17] ATLAS Collaboration, "Search for direct top squark pair production in final states with one isolated lepton, jets, and missing transverse momentum in $\sqrt{s}$ = 7 TeV pp collisions using 4.7 fb^{-1} of ATLAS data", *Phys. Rev. Lett.* **109** (2012) 211803, doi:10.1103/PhysRevLett.109.211803, arXiv:1208.2590.

[18] ATLAS Collaboration, "Search for a heavy top-quark partner in final states with two leptons with the ATLAS detector at the LHC", *JHEP* **1211** (2012) 094, doi:10.1007/JHEP11(2012)094, arXiv:1209.4186.

[19] CMS Collaboration, "Search for top-squark pair production in the single-lepton final state in pp collisions at $\sqrt{s} = 8$ TeV", arXiv:1308.1586. Accepted by *Eur. Phys. J. C*.

[20] CMS Collaboration, "Scalar Top Quark Search with Jets and Missing Momentum in pp Collisions at $\sqrt{s} = 7$ TeV", CMS Physics Analysis Summary CMS-PAS-SUS-11-030, (2013).

[21] CMS Collaboration, "Search for supersymmetry using razor variables in events with b-jets in pp collisions at 8 TeV", CMS Physics Analysis Summary CMS-PAS-SUS-13-004, (2013).

[22] CDF Collaboration, "Search for the supersymmetric partner of the top quark in $p\bar{p}$ collisions at $\sqrt{s}$ = 1.96 TeV", *Phys. Rev. D* **82** (2010) 092001, doi:10.1103/PhysRevD.82.092001, arXiv:1009.0266.

[23] D0 Collaboration, "Search for pair production of the scalar top quark in the electron+muon final state", *Phys. Lett. B* **696** (2011) 321, doi:10.1016/j.physletb.2010.12.052, arXiv:1009.5950.

[24] CMS Collaboration, "CMS Luminosity Based on Pixel Cluster Counting - Summer 2013 Update", CMS Physics Analysis Summary CMS-PAS-LUM-13-001, (2013).

[25] CMS Collaboration, "Search for new physics with jets and missing transverse momentum in pp collisions at $\sqrt{s} = 7$ TeV", *JHEP* **08** (2011) 155, doi:10.1007/JHEP08(2011)155, arXiv:1106.4503.

[26] CMS Collaboration, "Search for New Physics in the Multijet and Missing Transverse Momentum Final State in Proton-Proton Collisions at $\sqrt{s} = 7$ TeV", *Phys. Rev. Lett.* **109** (2012) 171803, doi:10.1103/PhysRevLett.109.171803, arXiv:1207.1898.

[27] CMS Collaboration, "Search for New Physics in the Multijets and Missing Momentum Final State in Proton-Proton Collisions at 8 TeV", CMS Physics Analysis Summary CMS-PAS-SUS-13-012, (2013).

[28] D. E. Kaplan, K. Rehermann, M. D. Schwartz, and B. Tweedie, "Top Tagging: A Method for Identifying Boosted Hadronically Decaying Top Quarks", *Phys. Rev. Lett.* **101** (2008) 142001, doi:10.1103/PhysRevLett.101.142001, arXiv:0806.0848.

[29] T. Plehn, M. Spannowsky, M. Takeuchi, and D. Zerwas, "Stop Reconstruction with tagged tops", *JHEP* **1010** (2010) 078, doi:10.1007/JHEP10(2010)078, arXiv:1006.2833.

[30] D. E. Kaplan, K. Rehermann, and D. Stolarski, "Searching for direct stop production in hadronic top data at the LHC", *JHEP* **1207** (2012) 119, doi:10.1007/JHEP07(2012)119, arXiv:1205.5816.

[31] CMS Collaboration, "The CMS experiment at the CERN LHC", *JINST* **0803** (2008) S08004, doi:10.1088/1748-0221/3/08/S08004.

[32] CMS Collaboration, "Particle Flow Event Reconstruction in CMS and Performance for Jets, Taus and MET", CMS Physics Analysis Summary CMS-PAS-PFT-09-001, (2009).

[33] M. Cacciari, G. P. Salam, and G. Soyez, "The anti-k_t jet clustering algorithm", *JHEP* **0804:063** (2008) doi:10.1088/1126-6708/2008/04/063, arXiv:0802.1189.

[34] M. Cacciari and G. P. Salam, "Pileup subtraction using jet areas", *Phys. Lett. B* **659** (2007) 119, doi:10.1016/j.physletb.2007.09.077, arXiv:0707.1378.

[35] M. Cacciari, G. P. Salam, and G. Soyez, "The catchment area of jets", *JHEP* **04** (2007) 005, doi:10.1088/1126-6708/2008/04/005, arXiv:0802.1188.

[36] CMS Collaboration, "Determination of jet energy calibration and transverse momentum resolution in CMS", *JINST* **6** (2011) P11002, doi:10.1088/1748-0221/6/11/P11002, arXiv:1107.4277.

[37] CMS Collaboration, "Performance of b tagging at $\sqrt{s} = 8$ TeV in multijet, $\mathrm{t\bar{t}}$ and boosted topology events", CMS Physics Analysis Summary CMS-PAS-BTV-13-001, (2013).

[38] CMS Collaboration, "Performance of muon identification in pp collisions at $\sqrt{s} = 7$ TeV", CMS Physics Analysis Summary CMS-PAS-MUO-10-002, (2010).

[39] J. Alwall et al., "MadGraph/MadEvent v4: the new web generation", *JHEP* **09** (2007) 028, doi:10.1088/1126-6708/2007/09/028, arXiv:0706.2334.

[40] T. Sjöstrand, S. Mrenna, and P. Z. Skands, "PYTHIA 6.4 physics and manual", *JHEP* **05** (2006) 026, doi:10.1088/1126-6708/2006/05/026, arXiv:hep-ph/0603175.

[41] R. Field, "Early LHC Underlying Event Data - Findings and Surprises", arXiv:1010.3558.

[42] J. Pumplin et al., "New Generation of Parton Distributions with Uncertainties from Global QCD Analysis", *JHEP* **07** (2002) 012, doi:10.1088/1126-6708/2002/07/012, arXiv:hep-ph/0201195.

[43] S. Frixione, P. Nason, and C. Oleari, "Matching NLO QCD computations with parton shower simulations: the POWHEG method", *JHEP* **11** (2007) 070, doi:10.1088/1126-6708/2007/11/070, arXiv:0709.2092.

[44] H.-L. Lai et al., "New parton distributions for collider physics", *Phys. Rev. D* **82** (2010) 074024, doi:10.1103/PhysRevD.82.074024, arXiv:1007.2241.

[45] P. M. Nadolsky et al., "Implications of CTEQ global analysis for collider observables", *Phys. Rev. D* **78** (2008) 013004, doi:10.1103/PhysRevD.78.013004, arXiv:0802.0007.

[46] K. Melnikov and F. Petriello, "Electroweak Gauge Boson Production at hadron colliders through $O(\alpha(s)^2)$", *Phys. Rev. D* **74** (2006) 114017, doi:10.1103/PhysRevD.74.114017, arXiv:hep-ph/0609070.

[47] R. Gavin, Y. Li, F. Petriello, and S. Quackenbush, "W physics at the LHC with FEWZ 2.1", *Comput. Phys. Commun.* **184** (2013) 208, doi:10.1016/j.cpc.2012.09.005, arXiv:1201.5896.

[48] N. Kidonakis, "Next-to-next-to-leading-order collinear and soft gluon corrections for *t*-channel single top quark production", *Phys. Rev. D* **83** (2011) 091503, doi:10.1103/PhysRevD.83.091503, arXiv:1103.2792.

[49] N. Kidonakis, "NNLL resummation for *s*-channel single top quark production", *Phys. Rev. D* **81** (2010) 054028, doi:10.1103/PhysRevD.81.054028, arXiv:1001.5034.

[50] N. Kidonakis, "Two-loop soft anomalous dimensions for single top quark associated production with a W^- or H^-", *Phys. Rev. D* **82** (2010) 054018, doi:10.1103/PhysRevD.82.054018, arXiv:1005.4451.

[51] N. Kidonakis, "Next-to-next-to-leading Soft-Gluon Corrections for the Top Quark Cross Section and Transverse Momentum Distribution", *Phys. Rev. D* **82** (2010) 114030, doi:10.1103/PhysRevD.82.114030, arXiv:1009.4935.

[52] N. Kidonakis, "Differential and total cross sections for top pair and single top production", in *XX International Workshop on Deep-Indelastic Scattering and Related Subjects*, p. 831. Bonn, 2012. arXiv:1205.3453. doi:10.3204/DESY-PROC-2012-02/251.

[53] M. V. Garzelli, A. Kardos, C. G. Papadopoulos, and Z. Trocsanyi, "$t\bar{t}W^{\pm}$ and $t\bar{t}Z$ Hadroproduction at NLO Accuracy in QCD with Parton Shower and Hadronization Effects", *JHEP* **11** (2012) 056, doi:10.1007/JHEP11(2012)056, arXiv:1208.2665.

[54] J. M. Campbell and R. K. Ellis, "$t\bar{t}W^{\pm}$ production and decay at NLO", *JHEP* **07** (2012) 052, doi:10.1007/JHEP07(2012)052, arXiv:1204.5678.

[55] J. M. Campbell and R. K. Ellis, "MCFM for the Tevatron and the LHC", *Nucl. Phys. Proc. Suppl.* **205-206** (2010) 10, doi:10.1016/j.nuclphysbps.2010.08.011, arXiv:1007.3492.

[56] CMS Collaboration, "The fast simulation of the CMS detector at LHC", *J. Phys. Conf. Ser.* **331** (2011) 032049, doi:10.1088/1742-6596/331/3/032049.

[57] J. Allison et al., "Geant4 developments and applications", *IEEE 53* **1** (2006) 270, doi:10.1109/TNS.2006.869826.

[58] CMS Collaboration, "Missing transverse energy performance of the CMS detector", *JINST* **6** (2011) P09001, doi:10.1088/1748-0221/6/09/P09001, arXiv:1106.5048.

[59] CMS Collaboration, "MET performance in 8 TeV data", CMS Physics Analysis Summary CMS-PAS-JME-12-002, (2013).

[60] C. G. Lester and D. J. Summers, "Measuring masses of semi-invisibly decaying particles pair produced at hadron colliders", *Phys. Lett. B* **463** (1999) 99, doi:10.1016/S0370-2693(99)00945-4, arXiv:hep-ph/9906349.

[61] A. Barr, C. Lester, and P. Stephens, "A variable for measuring masses at hadron colliders when missing energy is expected; m_{T2}: the Truth behind the glamour", *J. Phys. G* **29** (2003) 2343, doi:10.1088/0954-3899/29/10/304, arXiv:hep-ph/0304226.

[62] N. Davidson et al., "Universal Interface of TAUOLA Technical and Physics Documentation", *Comput. Phys. Commun.* **183** (2012) 821, doi:10.1016/j.cpc.2011.12.009, arXiv:1002.0543.

[63] Particle Data Group Collaboration, "Review of Particle Physics", *Phys. Rev. D* **86** (2012) 010001, doi:10.1103/PhysRevD.86.010001. http://pdg.lbl.gov.

[64] B. Efron, "The Jackknife, The Bootstrap and Other Resampling Plans", volume 38 of *CBMS-NSF Regional Conference Series in Applied Mathematics*. SIAM, Philadelphia, 1982.

[65] CMS Collaboration, "Tau identification in CMS", CMS Physics Analysis Summary CMS-PAS-TAU-11-001, (2011).

[66] CMS Collaboration, "Measurement of the inclusive W and Z production cross sections in pp collisions at $\sqrt{s} = 7$ TeV with the CMS experiment", *JHEP* **10** (2011) 132, doi:10.1007/JHEP10(2011)132, arXiv:1107.4789.

[67] M. Botje et al., "The PDF4LHC Working Group Interim Recommendations", arXiv:1101.0538.

[68] A. L. Read, "Presentation of search results: the CLs technique", *J. Phys. G* **28** (2002) 2693, doi:10.1088/0954-3899/28/10/313.

[69] T. Junk, "Confidence level computation for combining searches with small statistics", *Nucl. Instrum. Methods Phys. Res., Sect. A* **434** (1999) 435, doi:10.1016/S0168-9002(99)00498-2, arXiv:hep-ex/9902006.

[70] ATLAS and CMS Collaborations, "Procedure for the LHC Higgs boson search combination in Summer 2011", ATL-PHYS-PUB-2011-011, CMS NOTE-2011/005, (2011).

[71] W. Beenakker, R. Höpker, M. Spira, and P. M. Zerwas, "Squark and gluino production at hadron colliders", *Nucl. Phys. B* **492** (1997) 51, doi:10.1016/S0550-3213(97)00084-9.

[72] A. Kulesza and L. Motyka, "Threshold resummation for squark-antisquark and gluino-pair production at the LHC", *Phys. Rev. Lett.* **102** (2009) 111802, doi:10.1103/PhysRevLett.102.111802.

[73] A. Kulesza and L. Motyka, "Soft gluon resummation for the production of gluino-gluino and squark-antisquark pairs at the LHC", *Phys. Rev. D* **80** (2009) 095004, doi:10.1103/PhysRevD.80.095004.

[74] W. Beenakker et al., "Soft-gluon resummation for squark and gluino hadroproduction", *JHEP* **12** (2009) 041, doi:10.1088/1126-6708/2009/12/041.

[75] W. Beenakker et al., "Squark and gluino hadroproduction", *Int. J. Mod. Phys. A* **26** (2011) 2637, doi:10.1142/S0217751X11053560.

[76] M. Kramer et al., "Supersymmetry production cross sections in pp collisions at $\sqrt{s} = 7$ TeV", arXiv:1206.2892.